Chemical Methodologies 7(2023) 871-882

Chemical Methodologies

Journal homepage: http://chemmethod.com

Original Article

Studying the Structural and Optical Properties of Thin Compound Oxide Films Based on TiO_2: NiO: In_2O_3 Nanostructure

Fuad. T Ibrahim[1]*, M. Abd Shahoodh[2, 3], S. Guermazi[3]

[1]*Physics Department, College of Science, University of Baghdad, Baghdad, Iraq*
[2]*Ministry of Education, Anbar Education directorate, Anbar, Iraq*
[3]*Laboratory of Materials for Energy and Environment, and Modeling (LMEEM), Faculty of Sciences, University of Sfax, B.P: 1171, 3038, Tunisia*

ARTICLEINFO

Article history
Submitted: 2023-08-02
Revised: 2023-10-06
Accepted: 2023-11-15
Manuscript ID: CHEMM-2308-1693
Checked for Plagiarism: Yes
Language Editor:
Dr. Fatimah Ramezani
Editor who approved publication:
Dr. Hamid Saeidian

DOI:10.48309/chemm.2023.409731.1693

KEYWORDS
TiO_2/NiO/In_2O_3
Nanostructure
Gas sensor
H_2S gas

ABSTRACT

Spray pyrolysis has been used to fabricate different mixed TiO_2/NiO/In_2O_3 nanostructures. TiO_2/NiO/In_2O_3 has been structurally and optically explored using X-ray diffraction, field emission scanning electron microscopy, and UV-Vis spectroscopy. The particles analysis using X-ray diffraction had a polycrystalline structure and all of the observed peaks can be assigned to the samples with nanostructure, while FESEM reveals that they are very small, spherical, and range in size from 14 to 100 nm. The UV-Vis observed the edge of absorbance at about 335-305 nm; the energy band gap was calculated to be 3.3-3.58 eV. The absorbance in this area is caused by the creation of TiO_2/NiO/In_2O_3 nanoparticles. The synthesis of thin films was tested in gas sensor applications. The gas response of the tested samples to hydrogen sulfide gas at different operating temperatures was analysed. The thin film demonstrates that when the operating temperature got higher, sensitivity increased as well. With an increase in operational temperature, recovery and response times are slowed down.

* Corresponding author: Fuad .T Ibrahim
✉E-mail: fuadtariq1975@gmail.com

GRAPHICALABSTRACT

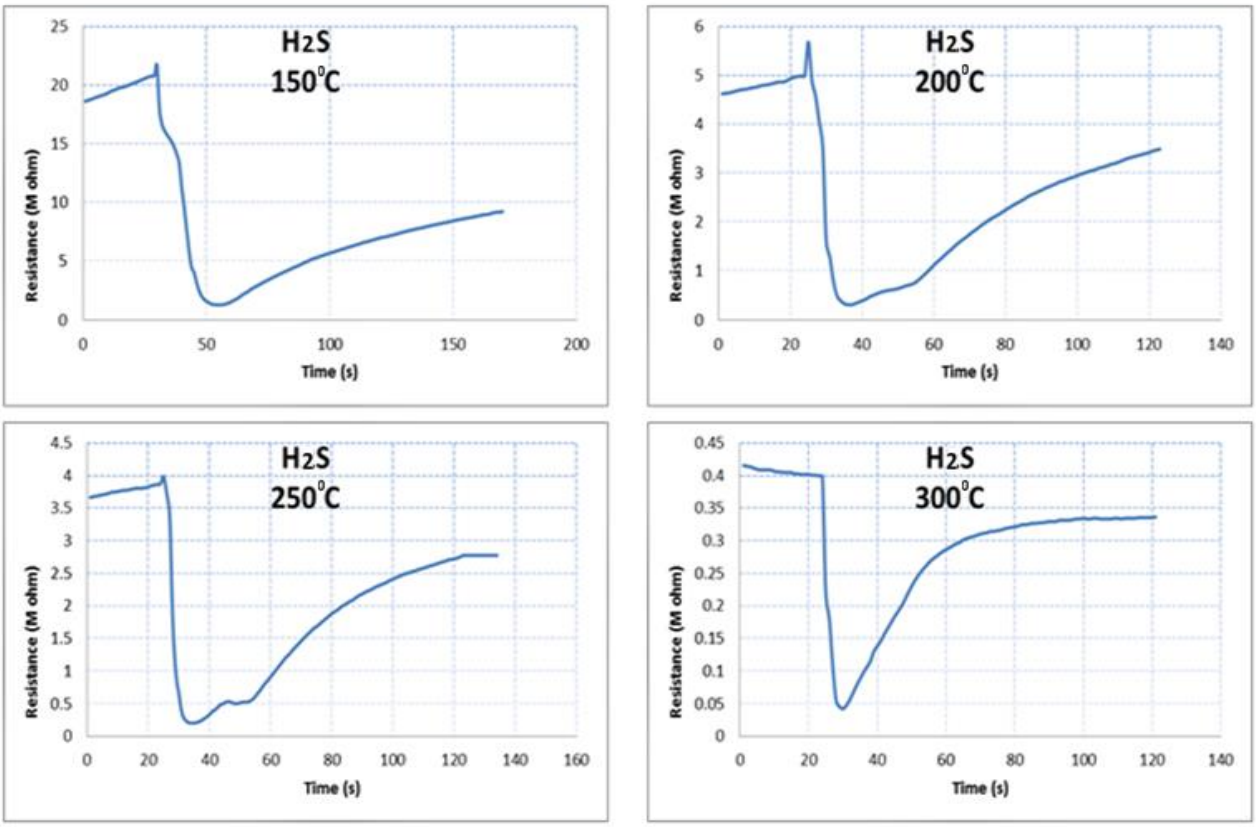

Introduction

Hydrogen sulfide gas (H_2S), which are combustible and toxic, are created by the sewage treatment, coal, oil, and natural gas sectors. H_2S was employed in a wide range of chemical industries, as well as in research facilities, and as a process gas in the manufacturing of heavy water. Although the gas's lateral exposure length is 10 ppm for an 8 h exposure, H_2S pleasant ambient scale is between 20 and 100 ppb [1].

It is therefore desirable to find H_2S at these small sizes. Low amounts of this gas can be detected by spectral and fluorescence analysis [2], but these sensors are expensive and have enormous dimensions. The most common kind of gas sensor that offers cheap cost, high sensitivity and selectivity, environmental friendliness, and portable device capabilities for long-range operations is thin film chemiresistive gas sensors based on transition metal oxides (TMOs) [3]. Transition metal oxide, which is used in optoelectronic devices including photodiodes, solar cells, and flat-panel displays, etc. The physical properties of transition metal oxide films created by various deposition techniques, such as laser deposition [4], molecular beam epitaxy [5], the sol-gel process [7], spray pyrolysis [8], dc/rf magnetron sputtering [9], and evaporation with electron beams [10], chemical vapour deposition [6], and electrochemical deposition [11] have been the focus of in-depth study for the past thirty years. In recent years, many researches have been conducted in the field of gas sensors using titanium dioxide [12], conductive polymers [13], nanoconductive polymers [14], nano cerium oxide/aluminum oxide [15], and nano cerium (IV) oxide/zinc oxide [16] all of which gave impressive results in the field of sensors. Where titanium dioxide can be applied in many fields, including an experimental study of the structural and photocatalytic properties of nitrogen-doped titanium dioxide [17], Au decorated mesoporous TiO_2 as a high performance photocatalyst towards crystal violet dye [18].

Also, some compounds other than titanium, such as single-phase bismuth nanoparticles ($BiFeO_3$), can be used in photocatalysts [19].

Finally, semiconductor nanoparticles have been used in many other applications, the most important of which is chemical catalysts [20-23].

In this work, the spray pyrolysis technique was used to fabricate thin films of $TiO_2/NiO/In_2O_3$ on glass substrates. Nanostructure, morphological and hydrogen sulfate gas sensing properties were investigated in detail.

Experimental

Materials and methods

The chemical spray pyrolysis technique was used to fabricate $NiO/TiO_2/In_2O_3$ nanostructure thin films on glass substrates heated to 400 °C, as depicted in Figure 1. Prior to the deposition, there was a predetermined 30 cm gap between the sprayer head and the substrate. Glass substrates with 2×2 cm^2 were cleaned using an ultrasonic cleaner for 15 min with acetone, ethanol, and deionized water, and then dried for an hour in an air oven at 100 °C.

Indium chloride ($InCl_3$), purity 99.99%, molecular weight 221.18 g/mole and nickel chloride ($NiCl_2$), quality 99.99%, molecular weight 129.5994 g/mole were used to prepared 0.2 M were dissolved in 100 ml of deionized water. A solution of 100 ml with 0.2 M titanium trichloride ($TiCl_3$), purity of 99.99%, molecular weight of 154.22 g/mole was also used. The solutions were mixed using a magnetic stirrer until completely dissolved, and the molarity (M) was calculated using the formula:

$M = (Wt / MW) \times (1000 / V)$ (1)

where, Wt is the wight of salt in gram, MW is the molar weight typically in gram per moles, and V is the volume of the solution typically in litres. $TiO_2/NiO/In_2O_3$ films with various molar ratios 2:6:2, 3:5:2, and 4:4:2were prepared. Using a home-made gas-detection device, the sensors' sensing abilities were tested. The base plate was the conduit for electrical feeds, the base plate's heating was modified in order to warm the test sample and bring it to the required operating temperatures. A thermocouple was used to determine the sensors' operating temperature.

Digital temperature displays were linked to the thermocouple's output, and one of the apertures on the base plate had a gas inlet valve attached to it. Using a gas flow meter, a known quantity of

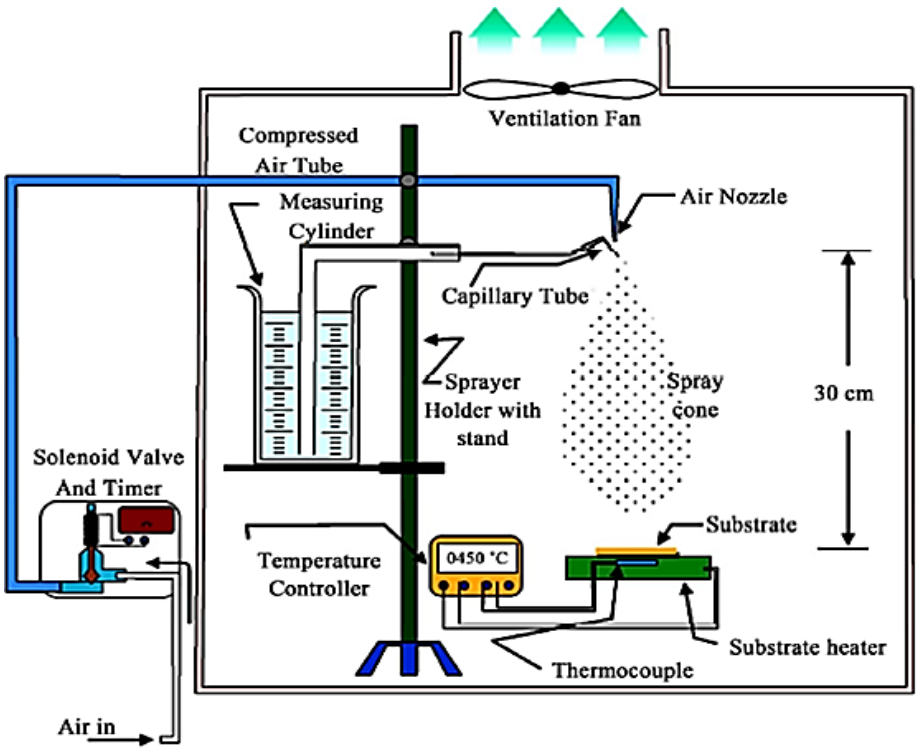

Figure 1: Schematic of spray pyrolysis technique

test gas was introduced into the system to create the desired gas concentration. A steady voltage and current were sent to the sensors.

FESEM (inspect F-50 company) was used for determining the morphology of the materials. XRD (6000 SHIMADZ made in Japan) was utilized for estimating crystal structure and the average crystallite size. UV-Vis absorption was measured using a Perkin Elmer Spectrophotometer Model Lambda 365.

Results and Discussion

The X- ray patterns of $TiO_2/NiO/In_2O_3$ thin films at varies concentration are shown in Figure 2, were prepared by spray pyrolysis technique. The samples were prepared on glass substrate at temperature 400 ºC, 30 cm distance between spray head and substrate and the scans were performed over 2θ=[10º-80º]. In general, can find that the samples had a polycrystalline structure and all of the observed peaks can be assigned to the samples, in accordance to the data obtained from JCPDF (card no. 21-1276) [24].

The formation of TiO_2 thin film and planes corresponding to (010), (200), (211), and (204) appear polycrystalline structure with tetragonal anatase phase. Start planes for the fabrication of nickel oxide crystals are (111) and (200) planes. The diffraction pattern of the sample, which were indicates the polycrystalline of the NiO thin film with nanostructure cubic phase. In addition, the show XRD patterns for In_2O_3 thin film exhibit a polycrystalline nature with (211), (222), (222), (400), and (440), planes with nanostructure cubic phase. Table 1, represent a full width at half maximum (FWHM), inter-planar distance (d_{hkl}) and the grain size (G.S.) using the Scherrer equation, the grain size was determined from FWHM (β) [25]. From the results, a smaller grain size as well as larger FWHM values mark preferable crystallization of the materials and nanocrystalline material can be grown by preparation condition.

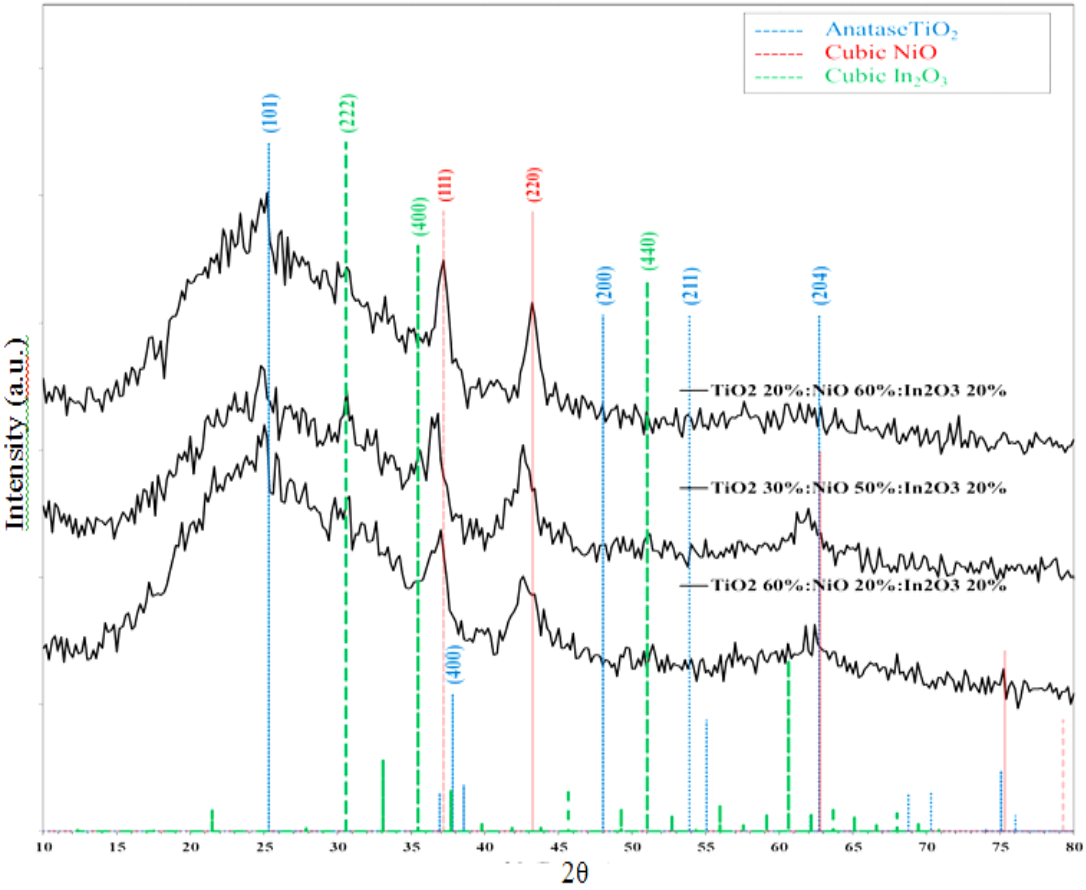

Figure 2: XRD of $TiO_2/NiO/In_2O_3$ composite thin films on glass substrate

Table 1: Comparison of the standard and expected values of d_{hkl} for the peaks identified by XRD

Sample	2θ (Deg.)	FWHM (radin)	d_{hkl} Exp.(Å)	D (nm)	Phase	hkl	card No.
TiO_2 40% NiO 40% In_2O_3 20%	25.0745	0.8419	3.54855	9.7	Anatase	(110)	96-900-9087
	30.5269	0.8420	2.92603	9.8	Cub.In_2O_3	(222)	96-101-0589
	36.9015	1.2027	2.43389	7.0	Cub. NiO	(111)	96-432-0488
	42.4742	1.3230	2.12656	6.4	Cub. NiO	(220)	96-432-0488
	51.4147	0.6414	1.77581	13.7	Cub.In_2O_3	(440)	96-101-0589
	62.4399	0.6816	1.48613	13.6	Anatase	(204)	96-900-9087
TiO_2 30% NiO 50% In_2O_3 20%	24.7938	0.8018	3.58809	10.1	Anatase	(110)	96-900-9087
	30.5670	0.8820	2.92228	9.3	Cub.In_2O_3	(222)	96-101-0589
	35.6586	0.7217	2.51582	11.6	Cub.In_2O_3	(400)	96-101-0589
	36.6609	0.9221	2.44931	9.1	Cub. NiO	(111)	96-432-0488
	42.5544	1.0424	2.12274	8.2	Cub. NiO	(220)	96-432-0488
	51.0538	0.8018	1.78751	11.0	Cub.In_2O_3	(440)	96-101-0589
	61.9989	1.3631	1.49564	6.8	Anatase	(204)	96-900-9087
TiO_2 20% NiO 60% In_2O_3 20%	25.0745	0.8820	3.54855	9.2	Anatase	(110)	96-900-9087
	30.4868	0.9221	2.92979	8.9	Cub.In_2O_3	(222)	96-101-0589
	37.1821	0.8821	2.41616	9.5	Cub. NiO	(111)	96-432-0488
	43.2360	1.0424	2.09084	8.2	Cub. NiO	(220)	96-432-0488

Nanoscale grass-like features are seen on the SEM image of the $TiO_2/NiO/In_2O_3$ thin films, as illustrated in Figure 3. The nanostructure is aligned and is homogeneously distributed with few vacancies.

Polyhedral shells are also scattered depressively over the surface, with some lining up along the nanoparticle. The SEM image shows small granular grains evenly scattered over the surface with no cracks. However, white-coloured spots developed on the film surface from time to time, possibly due to the partial breakdown of the precursor salt employed. Small spherical granules with sizes ranging from 20 to 100 nm were discovered. The film surface looks to be homogeneous, with no holes or breaks. However, XRD measurements show that the grain size is smaller than expected by the SEM surface micrograph.

In general, thin films of metal oxides are optically transparent and electrically conductive within the visible wavelength range. The optical measurement of the prepared films were carried out using UV-Vis (200-900) nm Spectroscope and the spectral dependence of the absorbance for all thin films deposit at same conditions, for different mixed TiO_2, NiO and In_2O_3 are demonstrated in Figure 4. The thin film absorbance spectra as a function of wavelength, in the range of 200-900 nm were analysed. There are three main zones of interest, as indicated by the spectral dependency in the Figure 4.

The existence of these oscillations is an indication of the films' high optical quality. When stored in an environment, all films were stable for a long time, uniformly adhered to the substrate, and transparent. The typical absorbance of films formed on glass substrates is higher by around 0.1 over the wavelength range 400 to 800 nm. A sharp fall in absorption at about 335, 325, and 305 nm is due to absorption edge of different mixed TiO_2 (40, 30, and 20)%: NiO(40, 50, and 60)%: In_2O_3 20% semiconductor thin films, respectively.

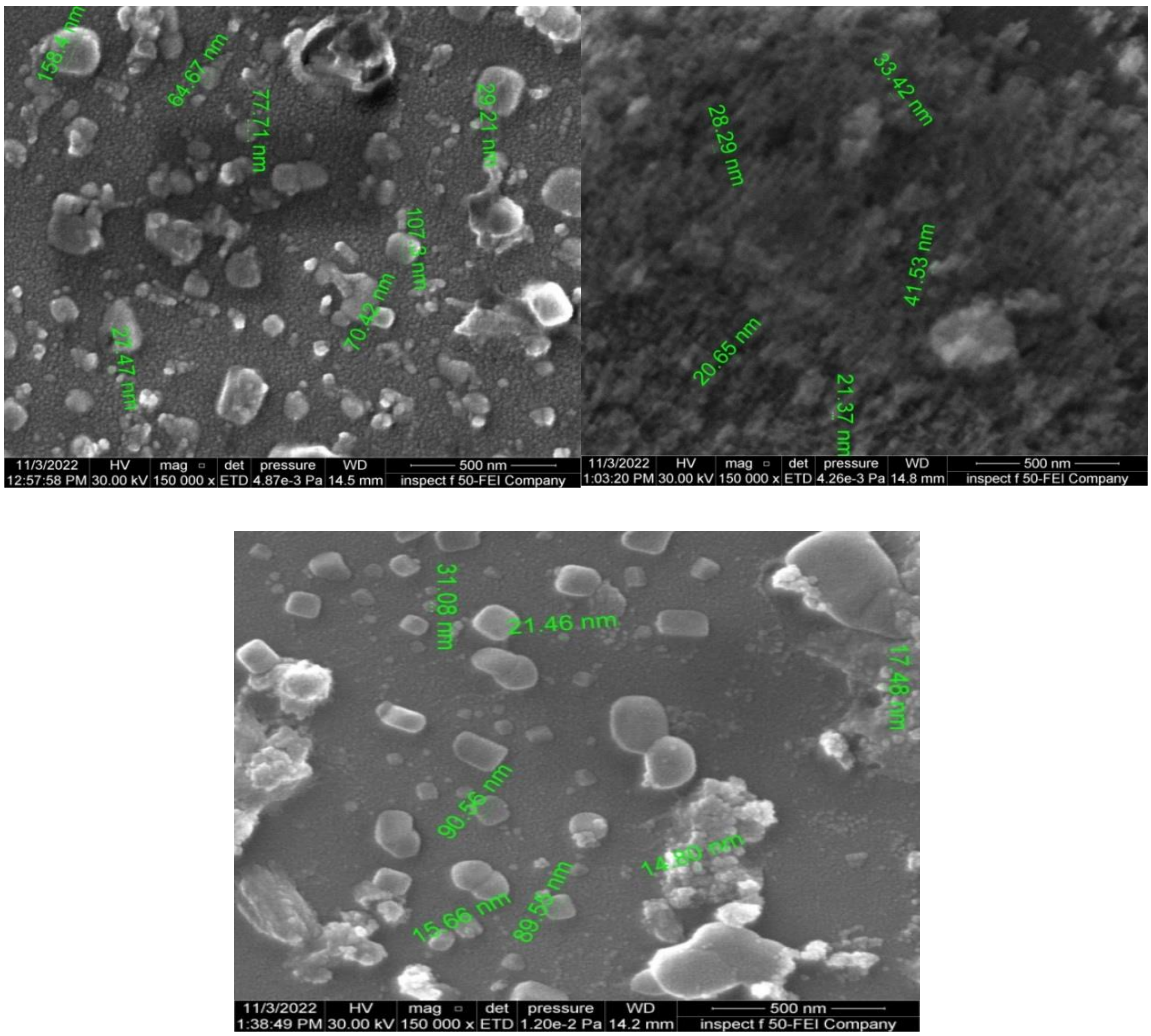

Figure 3: The FESEM images of $TiO_2/NiO/In_2O_3$ hin film deposited on glass substrate

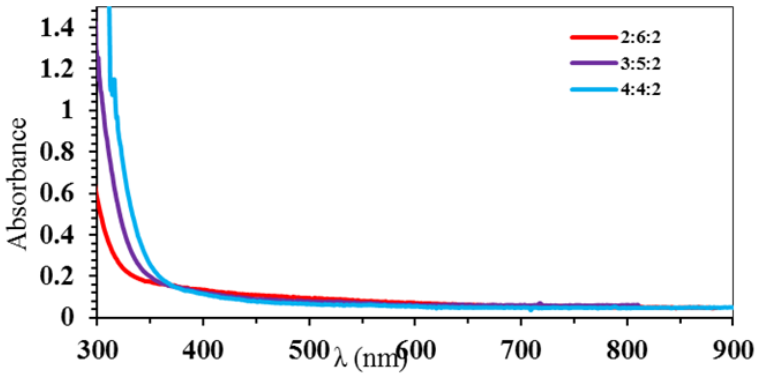

Figure 4: Absorbance spectrum as a function of wavelength for different mixed $TiO_2/NiO/In_2O_3$

The absorption edge was slightly red shifted with the increasing mixed ratio of TiO_2 respect to NiO, as depicted in Figure 4. One can calculate the semiconductor's band gap (E_g) using the data point close to the absorption edge. The absorption coefficient (α) for directly permitted transitions on basic parabolic scale can be expressed as αhυ various $(h\upsilon\text{-}E_g)^{1/2}$ as a function of incident photon energy. By extrapolating the graph's straight line to the energy axis, the band gap can be calculated. Table 2 presents the optical energy gap values for all samples in vest verse. A significant degree of non-stoichiometric abnormalities in the film may be the root of the

Table 2: Parameter of different mixed $TiO_2/NiO/In_2O_3$ thin films

$TiO_2/NiO/In_2O_3$	T%	α (cm^{-1})	K	N	ε_r	ε_i	Eg (eV)
2:6:2	92.82	11170	0.044	1.496	2.235	0.132	3.58
3:5:2	94.04	9212	0.037	1.443	2.081	0.106	3.43
4:4:2	95.21	7370	0.031	1.390	1.931	0.086	3.3

Table 3: The activation energy of different mixed $TiO_2/NiO/In_2O_3$

mixed samples	E_{a1} (eV)	Range (K)	E_{a2} (eV)	Range (K)	σ_{RT} *10^{-7}(Ω^{-1}.cm^{-1})
2:6:2	0.281	303-393	0.523	393-473	20.76
3:5:2	0.257	303-393	0.520	393-473	20.29
4:4:2	0.184	303-393	0.580	393-473	19.84

relatively high band gap value. This implies that the high conducting electron density is due to defects from the ideal single crystal structure, such as oxygen vacancies, interstitial atoms, and dislocations acting as conducting electron donors. The metal component oxidation state (also known as the stoichiometry of the oxide), the kind and quantity of mixture included in the thin films have significant effects on the electrical characteristics of metal oxide. The mobility (μ), concentration (n), and of the specific free carrier, are all related to electrical conductivity (σ). For the production of thin films with high conductivity, both high carrier concentration and mobility are necessary [26]. Likewise, the morphology of the samples has a major effect on the electrical properties [27]. As oxygen vacancies get larger in amount, electrical conductivity becomes greater [28]. For nanometric grains with a little contribution at the grain boundary, electrical conductivity is higher. In contrast to bulk material grains, where the (σ) is linked to trapped carriers at the grain boundary, in this instance, the high (σ) is connected to the uniform distribution of carriers throughout the grain [29]. The grain boundary effect makes up a small portion of the total conductivity, whereas the electron mobility within the grain makes up the majority of the electrical conductivity. The maximum value of the activation energy during the low temperature area is caused by a modest amount of thermal energy that is more than enough to activate the charge carriers that occur during the conduction process. This activation energy grows as the operation temperature for samples rises. In contrast, a rise in charge mobility can be credited with the increased conductivity in the low temperature area. When compared to regions with low temperatures, activation energy is higher in high temperature areas. In this area, intrinsic flaws known as high temperature or intrinsic conduction are the primary determinants of electrical conductivity. Table 3 provides an overview of activation energy variation for mixed thin films.

Figure 5 demonstrates the sensitivity of the $TiO_2/NiO/In_2O_3$ thin films coated on glass substrate as a function of temperature for H_2S gas, at operating temperature 150, 200, 250, and 300 ºC using reducing gas H_2S with 30 ppm concentration. According to this figure, a good sensitivity at must operating temperature 150 to 300 °C and it can be observed that it has the higher sensitivity to 30 ppm from H_2S, for temperature up to 200 °C was about 93.5 for a sample 40:40:20%. The increasing number of surface-adsorbed oxygen species and their nanoscale size are responsible for the enhanced sensitivity.

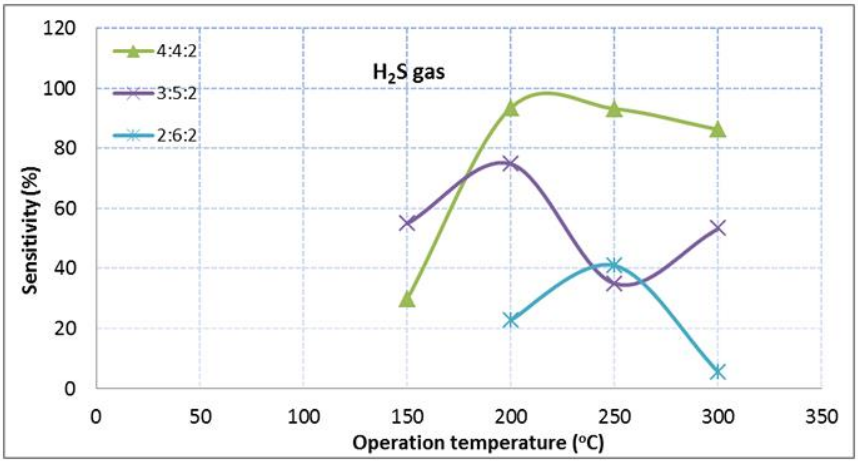

Figure 5: The variation of sensitivity with the operating temperature of the prepared, different mixed $TiO_2/NiO/In_2O_3$ to H_2S gas

Figure 6, demonstrates the response and recovery times for various mixed $TiO_2/NiO/In_2O_3$ as sensor samples as a function of temperature for H_2S gas. Figure 6 shows the response and recovery time decrease with increased the operation temperature. Where, the sample 4:4:2 thin film gas sensors have 6.3 s a fast response time for H_2S gas at 300 °C operation temperature, while the have fast recovery time 38.7 s for NO_2 gas at 300 °C operation temperature.

The surface reaction between chemisorbed oxygen and oxide gas is a key component of the gas sensing mechanism. There are two distinct methods by that oxygen can adsorb on a film surface: physisorption and chemisorption, where chemisorption predominates at high temperatures. Increasing operational temperature can provide the activation energy necessary for the transition from physisorption to chemisorption. According to reports, the amount of oxygen adsorbed on the sensor surface rises together with the temperature [30-31]. At temperatures between 150 and 300 °C, oxygen has a major impact on the electrophysical and gas sensing characteristics of samples where it is adsorbed at the surface of the metal oxide that permits an electron trapping. A location where the metal oxide's surface has oxygen adsorbed, allowing for the trapping of an electron. The result is a decrease in the charge carrier density, which raises the samples' resistance. O^- species on the surface serve as electron acceptors, causing a depletion layer to form that extends to the particles and the surface

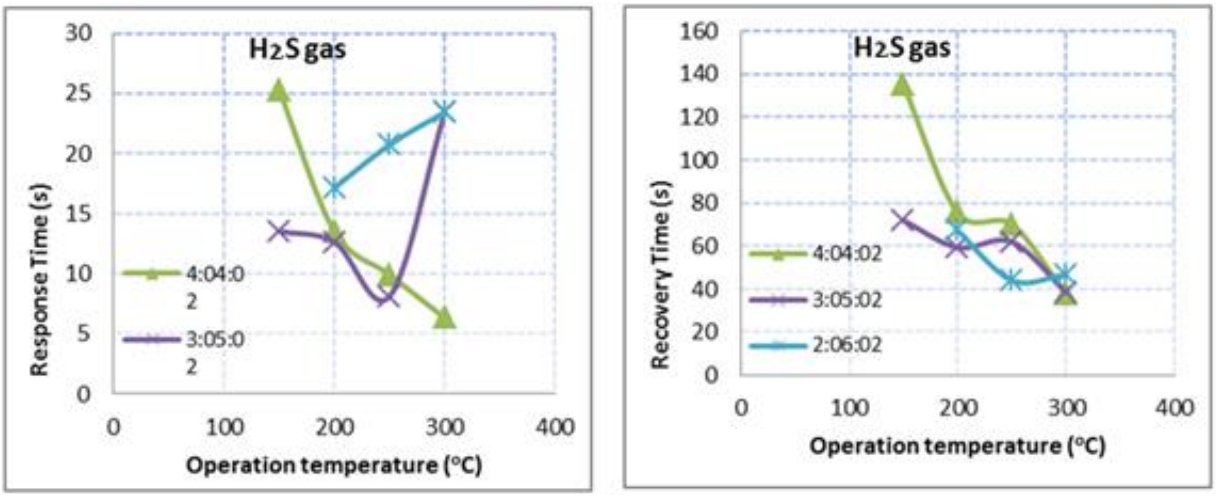

Figure 6: The variation of response time and recovery time with operation temperature of the prepared, different mixed $TiO_2/NiO/In_2O_3$ to H_2S gas

barrier, where, it regulates the electron transfer between particles, test gas, and the sensing material, and so affects the overall resistance, these surface states and surface barriers play a significant role for sensors. When exposed to H_2S gas at a high temperature, the pre-adsorbed oxygen species ($O^{-}surf$) are formed. It causes the oxygen coverage to increase, attracting more electrons to the samples conduction band and therefore increasing the barrier. This process reduces the depletion region and either increases resistance or reduces conductivity [32].

Figure 7 depicts the change in resistance as time progresses of $TiO_2/NiO/In_2O_3$ (40:40:20)% thin film as H_2S gas is fed into the testing chamber while the bias voltage is maintained at 3 V. The sensor resistance is directly correlated to time and initially reaches steady state prior to gas opening. At this point, the gas is opened to allow for air mixing inside the chamber. When switched the gas off, the resistance quickly reduced to achieve a stable condition before returning to its initial value. The way that gas molecules interact with the surface atoms of the detecting film determines how effectively a sensor can detect the presence of gas. The surface's reactivity is extremely reliant on the structural defect. When the gas is on, the resistance rapidly decreases over time until it reaches a saturated condition; this could be the result of the surface becoming saturated with H_2S gas adsorption. When the gas is turned off, the resistance returns to its initial state.

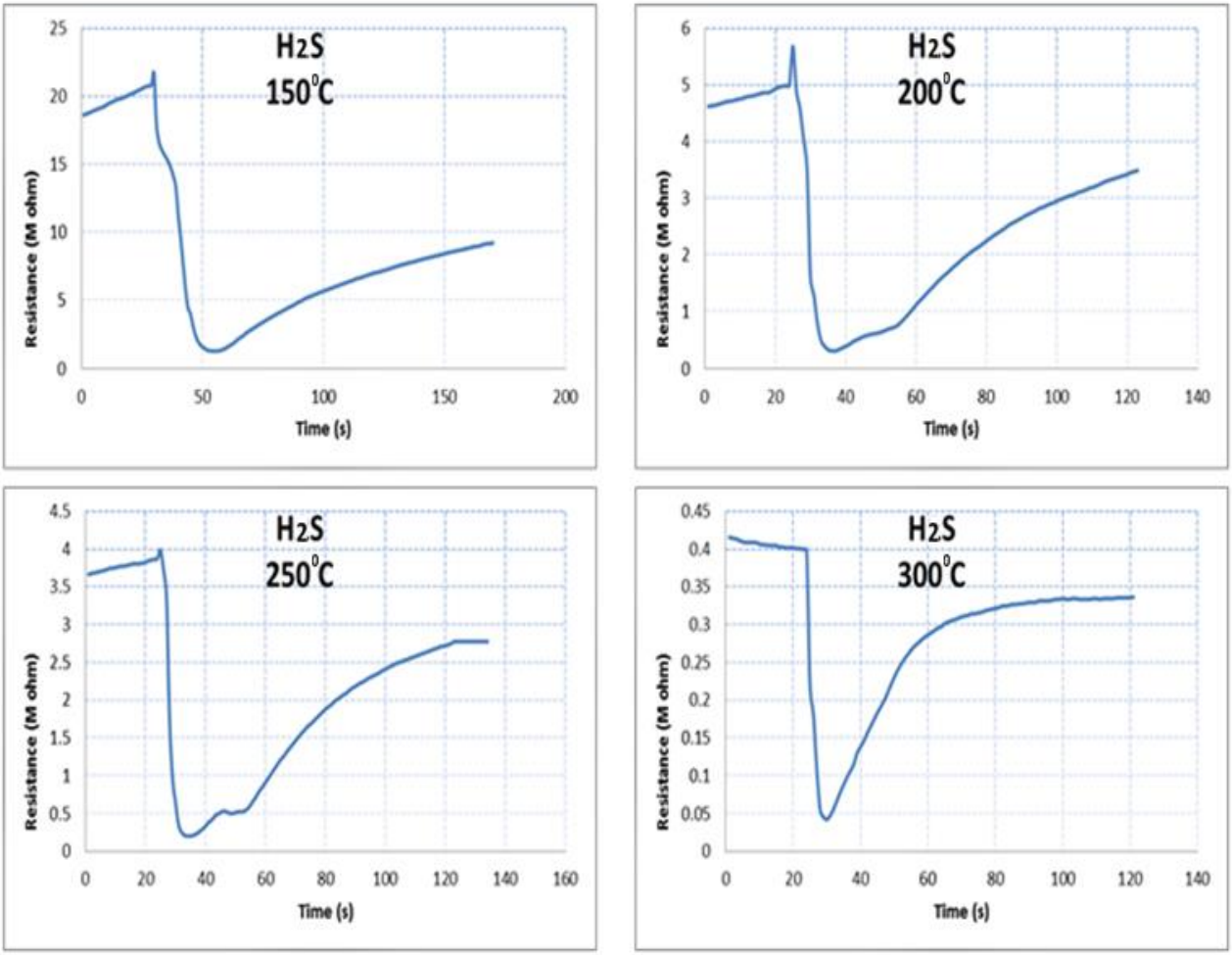

Figure 7: The variation resistance with time for different operation temperatures of H_2S gas for mixed TiO_2 40%: NiO 40%: In_2O_3 20% gas sensor

Conclusion

In conclusion, we have successfully constructed extremely sensitive $TiO_2/NiO/In_2O_3$ nanostructure thin film sensors for detecting trace amounts of H2S gas using the spray pyrolysis process. The $TiO_2/NiO/In_2O_3$ nanostructure thin film sensor demonstrated a high sensitivity value of 93.5% at 200C and a rapid response-recovery time of 6.3 s and 38.7 s at 300 oC for 4:4:2 thin film gas sensor sample. As a result, it is possible that the investigated thin film nanostructure will make it easier to find a suitable material for detecting low levels of H_2S in the environment. This work, therefore, provides a practical approach to the design and development of high-performance and low-power gas sensors.

Disclosure Statement

No potential conflict of interest was reported by the authors.

Funding

This study did not receive any specific grant from funding agencies in the public, commercial, or not-for-profit sectors.

Authors' contributions

All authors contributed toward data analysis, drafting, and revising the paper and agreed to responsible for all the aspects of this work.

Conflict of interest

The authors declare that they have no conflicts of interest in this article.

ORCID

Fuad .T Ibrahim
https://orcid.org/0000-0001-9796-9990

References

[1]. Kaur M., Jain N., Sharma K., Bhattacharya S., Roy M., Tyagi A., Gupta S., Yakhmi J., Room-temperature H2S gas sensing at ppb level by single crystal In_2O_3 whiskers, *Sensors and Actuators B: Chemical*, 2008, **133**:456 [Crossref], [Google Scholar], [Publisher]

[2]. Shete R., Fernandes P., Borhade B., Pawar A., Sonawane M., warude N., Review of Cobalt Oxide Nanoparticles: Green Synthesis, Biomedical Applications, and Toxicity Studies, *Journal of Chemical Reviews*, 2022, **4**:331 [Crossref], [Publisher]

[3]. Sanger A., Kumar A., Kumar A., Chandra R., Highly sensitive and selective hydrogen gas sensor using sputtered grown Pd decorated MnO2 nanowalls, *Sensors and Actuators B: Chemical*, 2016, **234**:8 [Crossref], [Google Scholar], [Publisher]

[4]. Yousif A.A., Hasan M.H., Gas sensitivity and morphologically characterized of nanostructure CdO doped In2O3 films deposited by pulsed laser deposition, *Journal of Biosensors Bioelectronics*, 2015, **6**:4 [Google Scholar], [Publisher]

[5]. Show V., Evaluating the quality of epitaxial In_2O_3 grown by suboxide molecular beam epitaxy. [PDF], [Google Scholar]

[6]. Taguchi A., Takahashi S., Sekiguchi A., Kaneko K., Fujita S., Onuma T., Honda T., Yamaguchi T., Mist Chemical Vapor Deposition Growth of α-In2O3 Films Using Indium Oxide Powder as Source Precursor, *physica status solidi (b)*, 2022, **259**:2100414 [Crossref], [Google Scholar], [Publisher]

[7]. Palomares-Sanchez S.A., Watts B.E., Klimm D., Baraldi A., Parisini A., Vantaggio S., Fornari R., Sol-gel growth and characterization of In2O3 thin films, *Thin Solid Films*, 2018, **645**:383 [Crossref], [Google Scholar], [Publisher]

[8]. Prince J.J., Ramamurthy S., Subramanian B., Sanjeeviraja C., Jayachandran M., Spray pyrolysis growth and material properties of In2O3 films, *Journal of Crystal Growth*, 2002, **240**:142 [Crossref], [Google Scholar], [Publisher]

[9]. Steffes H., Imawan C., Solzbacher F., Obermeier E., Fabrication parameters and NO2 sensitivity of reactively RF-sputtered In2O3 thin films, *Sensors and Actuators B: Chemical*, 2000, **68**:249 [Crossref], [Google Scholar], [Publisher]

[10]. Park S., Kim S., Sun G.J., Choi S., Lee S., Lee C., Ethanol sensing properties of networked In2O3 nanorods decorated with Cr2O3-nanoparticles, *Ceramics International*, 2015, **41**:9823 [Crossref], [Google Scholar], [Publisher]

[11]. Prasad K.R., Koga K., Miura N., Electrochemical deposition of nanostructured indium oxide: high-performance electrode material for redox supercapacitors, *Chemistry of Materials*, 2004, **16**:1845 [Crossref], [Google Scholar], [Publisher]

[12]. Rzaij J.M., Abass A.M., Review on: TiO_2 thin film as a metal oxide gas sensor, *Journal of Chemical Reviews*, 2020, **2**:114 [Google Scholar], [Publisher]

[13]. Agobi A.U., Louis H., Magu T.O., Dass P.M., A review on conducting polymers-based composites for energy storage application, *Journal of Chemical Reviews*, 2019, **1**:19 [Google Scholar], [Publisher]

[14]. Awan M.N., Razzaq H., Abid O.U., Qaisar S., Recent Advances in Electroanalysis of Hydrazine by Conducting Polymers Nanocomposites: A Review, *Journal of Chemical Reviews*, 2023, **5**:311 [Crossref], [Publisher]

[15]. Baghernejad B., Alikhani M., Nano-cerium oxide/aluminum oxide as an efficient catalyst for the synthesis of xanthene derivatives as potential antiviral and anti-inflammatory agents, *Quarterly Journal of Iranian Chemical Communication*, 2020, **8**:240 [Crossref], [Google Scholar], [Publisher]

[16]. Baghernejad B., Preparation of polyhydroquinolines in the presence of nano cerium (IV) oxide/zinc oxide as an efficient catalyst, *Journal of Applied Organometallic Chemistry*, 2022, **2**:74 [Crossref], [Google Scholar], [Publisher]

[17]. Rad F.A., Mehrabad J.T., Esrafili M.D., A Communal Experimental and DFT Study on Structural and Photocatalytic Properties of Nitrogen-Doped TiO2, 2023 [Crossref], [Google Scholar], [Publisher]

[18]. Darzi S.J., Bastami H., Au decorated mesoporous TiO_2 as a high performance photocatalyst towards crystal violet dye, *Advanced Journal of Chemistry section A*, 2022, **5**:22 [Crossref], [Google Scholar], [Publisher]

[19]. Ghahfarokhi S.M., Helfi K., Shoushtari M.Z., Synthesis of the single-phase bismuth ferrite (BiFeO3) nanoparticle and investigation of their structural, magnetic, optical and photocatalytic properties, *Advanced Journal of Chemistry-Section A*, 2022, **5**:45 [Crossref], [Google Scholar], [Publisher]

[20]. a) Heidaripour A., Synthesis of Coral-Like ZnO Nanostructures with High and Wide Absorption Range, 2023 [Google Scholar] b) Kavade R., Khanapure R., Gawali U., Patil A., Patil S., Degradation of Methyl Orange Under Visible Light by ZnO-Polyaniline Nanocomposites, *Journal of Applied Organometallic Chemistry*, 2022, **2**:89 [Crossref], [Publisher] c) Hajinasiri R., Esmaeili Jadidi M., Synthesis of ZnO Nanoparticles via Flaxseed Aqueous Extract, *Journal of Applied Organometallic Chemistry*, 2022, **2**:101 [Crossref], [Publisher]

[21]. a) Banifatemeh F., Polymerization of graphite and carbon compounds by aldol condensation as anti-corrosion coating, *Asian Journal of Green Chemistry*, 2023, **7**:25 [Crossref], [Google Scholar], [Publisher] b) Johnson A., Investigating the Effects of Environmental Applications on Decomposition of Zein Nanoparticles in Adsorbents in Industry, *Journal of Engineering in Industrial Research*, 2023, 4:93 [Crossref], [Publisher] c) Noor S., Al-Shamari A., High photocatalytic performance of ZnO and ZnO/CdS nanostructures against reactive blue 4 dye, *Journal of Medicinal and Pharmaceutical Chemistry Research*, 2023, 5: 776 [Publisher] d) Heidaripour A., Salmani F., Barati T., Synthesis of Coral-Like ZnO Nanostructures with High and Wide Absorption Range, *Asian Journal of Green Chemistry*, 2023, **7**:140 [Crossref], [Publisher]

[22]. a) Kallappa P.K.J., Kalleshappa P.G., Basavarajappa S., Eshwarappa B.B., Green synthesis of nanocellulose fibers from ragi stalk and its characterization, *Asian Journal of Green Chemistry*, 2022, **6**:273 [Crossref], [Google Scholar], [Publisher] b) Ullah R., Semiconductor ZnFe2O4 as Efficient Photocatalyst for the Degradation of Organic Dyes: An Update, *Journal of Chemical Reviews*, 2023, **5**:466 [Crossref], [Publisher]

[23]. Hakimi F., Golrasan E., Zinc sulfide (ZnS) nanoparticles: an effective catalyst for synthesis of benzoxazole derivatives, *Asian Journal of Green Chemistry*, 2023, **7**:47 [Crossref], [Google Scholar], [Publisher]

[24]. Dewi H.P., Santoso J., Trianda N.F., Rodiansono R., Synthesis and Characterization of Ag@ C-TiO2 Nanocomposite for Degradation of Sasirangan Textile Wastewater, *Jurnal Kimia*

Sains dan Aplikasi, 2019, **22**:299 [Crossref], [Google Scholar], [Publisher]

[25]. Rusu D., Rusu G., Luca D., Structural characteristics and optical properties of thermally oxidized zinc films, *Acta physica polonica A*, 2011, **119**:850 [Google Scholar]

[26]. Calnan S., Tiwari A., High mobility transparent conducting oxides for thin film solar cells, *Thin Solid Films*, 2010, **518**:1839 [Crossref], [Google Scholar], [Publisher]

[27]. Rahman M.M., Khan M., Islam M.R., Halim M., Shahjahan M., Hakim M., Saha D.K., Khan J.U., Effect of Al doping on structural, electrical, optical and photoluminescence properties of nano-structural ZnO thin films, *Journal of Materials Science & Technology*, 2012, **28**:329 [Crossref], [Google Scholar], [Publisher]

[28]. Ali H., Raaif M., Plasma oxidation of electron beam evaporated cadmium thin films, *Thin Solid Films*, 2012, **520**:4418 [Crossref], [Google Scholar], [Publisher]

[29]. Lamb D., Irvine S., Near infrared transparent conducting cadmium oxide deposited by MOCVD, *Thin Solid Films*, 2009, **518**:1222 [Crossref], [Google Scholar], [Publisher]

[30]. Shankar P., Rayappan J.B.B., Gas sensing mechanism of metal oxides: The role of ambient atmosphere, type of semiconductor and gases-A review, *Science Letters Journal,* 2015, **4**:126 [Google Scholar], [Publisher]

[31]. Salunkhe R., Shinde V., Lokhande C., Liquefied petroleum gas (LPG) sensing properties of nanocrystalline CdO thin films prepared by chemical route: effect of molarities of precursor solution, *Sensors and Actuators B: Chemical*, 2008, **133**:296 [Crossref], [Google Scholar], [Publisher]

[32]. Ansari Z., Ko T.G., Oh J.H., CO-sensing properties of In/sub 2/O/sub 3/-doped SnO/sub 2/thick-film sensors: effect of doping concentration and grain size, *IEEE Sensors Journal*, 2005, **5**:817 [Crossref], [Google Scholar], [Publisher]

HOW TO CITE THIS ARTICLE

Fuad .T Ibrahim*, M. Abd Shahoodh, S. Guermazi. Studying the Structural and Optical Properties of Thin Compound Oxide Films Based on TiO_2: NiO: In_2O_3 Nanostructure. *Chem. Methodol.*, 2023, 7(11) 871-882

DOI: https://doi.org/10.48309/chemm.2023.409731.1693

URL: https://www.chemmethod.com/article_183275.html